A Joint Constrained CCA Model for Network-Dependent Brain Subregion Parcellation: Supplementary Material

Qinrui Ling[1], Aiping Liu[1], Yu Li[1], Xueyang Fu[2], Xun Chen[1], Martin J. McKeown[3], and Feng Wu[1]

[1] *Department of Electronic Engineering and Information Science, University of Science and Technology of China, Hefei, China*

[2] *Department of Automation, University of Science and Technology of China, Hefei, China*

[3] *Department of Medicine, University of British Columbia, Vancouver, Canada*

I. NYU DATA

A. Participants and Data Acquisition

Twenty-five right-handed participants (fifteen males and ten females, range 21–49 years old) were included with no history of psychiatric or neurological disorders, which was confirmed by a psychiatric clinical assessment. Each subject had three sessions of resting-state fMRI data. The experiments were approved by the local Ethics Board, and written informed consent forms were obtained from all participants before the study.

A SIEMENS Allegra 3.0 Tesla scanner equipped for echoplanar imaging (EPI) was used for data acquisition. During the scans, participants were instructed to stay rest with their eyes open. Each participant was collected three resting-state scans of 197 continuous EPI functional volumes with the following specifications: repetition time of 2000 ms, echo time of 25 ms, flip angle of 90°, axial slices of 39 layers, matrix size of 64×64, field of view of 192 mm$\times$192 mm, and acquisition voxel size of 3.0 mm $\times$ 3.0 mm $\times$ 3.0 mm. Scans 2 and 3 were conducted in a single scan session, about 30 minutes apart, and were 5-11 months after scan 1. For spatial localization and normalization, a high-resolution T1-weighted anatomical image was also obtained using a magnetization prepared gradient echo sequence with repetition time of 2500 ms, echo time of 4.35 ms, inversion time of 900 ms, and flip angle = 8°. Additionally, as complete cerebellar coverage was impossible for all participants, only those cerebellar regions acquired in all participants were included in subsequent analyses.

B. fMRI Data Preprocessing

The acquired rs-fMRI data was preprocessed by DPABI (version 3.0, http://rfmri.org/dpabi) and SPM8 (https://www.fl.ion.ucl.ac.uk/spm). The first five time points were removed to make the magnetization dynamic stabilization, and slice timing correction was performed. The manually reoriented functional images were then co-registered to structural images, and were normalized to the Montreal Neurological Institute (MNI) space at $3.0 \times 3.0 \times 3.0\ mm^3$ resolution. Next, nuisance time courses

Table S1

THE ROIS SELECTED IN NYU DATA

No.	Name	No.	Name
1:2	Precentral	49:54	Occipital
3:16	Frontal	55:56	Fusiform
17:18	Rolandic_Oper	57:58	Postcentral
19:20	Supp_Motor_Area	59:62	Parietal
21:22	Olfactory	63:64	SupraMarginal
23:26	Frontal	65:66	Angular
27:28	Rectus	67:68	Precuneus
29:30	Insula	69:70	Paracentral_Lobule
31:36	Cingulum	71:72	Caudate
37:38	Hippocampus	73:74	Putamen
39:40	ParaHippocampal	75:76	Pallidum
41:42	Amygdala	77:78	Thalamus
43:44	Calcarine	79:80	Heschl
45:46	Cuneus	81:90	Temporal
47:48	Lingual	91:108	Cerebellum

Each region is suffixed by left(L), right(R), sup, mid, or inf according to its location.

were regressed from the processed data including head-motion parameters, linear trend, white-matter signal, and cerebrospinal fluid signal. Finally, fMRI signals were spatially smoothed using $6 \times 6 \times 6$ FWHM, and bandpass filtered between 0.01 to 0.08 Hz. To define the subregions in the Putamen, 106 other ROIs were selected as reference ROIs for generating the connectivity patterns of the Putamen, as shown in Table S1.

C. Results

1) Subregions of the Putamen: To better evaluate the reproducibility of the proposed model, we assessed its performance on the repeated sessions of resting-state fMRI data. For fair comparisons, all the subjects were registered in the common space. We parcellated the left and right Putamen separately, whose numbers of voxels were 306 and 322 respectively. 106 ROIs were chosen as reference regions to establish the connectivity patterns with the Putamen and guide its parcellation. Here, we set the number of subregions $K = 3$. Suppose that the defined subregions were spatially continuous whereas the reference ROIs did not require spatial continuity but required the sparsity of loadings. The Laplacian matrix was generated by the distance matrix of each voxel in the Putamen in 3-D Euclidean space, to reflect the spatial continuity of voxels. The tuning parameters $\beta_1, \beta_2, \gamma_1$ were chosen using 5-fold cross validation as $\beta_1 = 0.01, \beta_2 = 2.5, \gamma_1 = 0.01$. As an iterative method was adopted to solve

Table S2

THE SIGNIFICANTLY CORRELATED REFERENCE ROIS WITH THE LEFT PUTAMEN

	subregion 1	subregion 2	subregion 3
session 1	Insula_L	Precentral_R	Frontal_Inf_Oper_L
	Amygdala_L&R	Rolandic_Oper_L&R	Frontal_Inf_Tri_L&R
	Pallidum_L&R	Postcentral_L&R	Frontal_Inf_Orb_L&R
	Thalamus_L&R	Temporal_Sup_R	Parietal_Inf_L
session 2	Insula_L	Rolandic_Oper_L&R	Olfactory_L&R
	Amygdala_L&R	SupraMarginal_L	Frontal_Med_Orb_L
	Pallidum_L&R	Temporal_Sup_L&R	Caudate_L&R
	Thalamus_L&R		
session 3	Insula_L	Precentral_L&R	Olfactory_L&R
	Cingulum_Mid_L	Rolandic_Oper_R	Cingulum_Ant_L
	Amygdala_L&R	Supp_Motor_Area_R	Caudate_L&R
	Pallidum_L&R	Postcentral_L&R	
	Thalamus_L&R	Temporal_Sup_R	

the problem, it might fall into local rather than global minimum. We thus repeated the experiments 100 times with randomly initialized values and chose the one with the smallest loss function. After obtaining the canonical correlation loadings by JC-CCA, we derived the soft parcellation indicated by u_i and the corresponding significantly correlated reference ROIs by v, as shown in Table S2 and Table S3.

As demonstrated in the tables, for different sessions, the correlated reference ROIs were similar. For visualization, we selected the largest 30% weights of each u_i, and used the corresponding voxels to constitute a subregion. The parcellation results of one typical subject are illustrated in Fig. S1. For the left Putamen, subregion 1 was located in the inferior anterior part, subregion 2 mainly occupied the posterior part, and subregion 3 was located in the anterior part. For the right Putamen, subregion 1 was located in the inferior part, subregion 2 was located in the inferior part, and subregion 3 was located in the superior part. As we parcellated the left and right Putamen separately, the asymmetry was observed in both the parcellation results and their subregional connectivity patterns.

2) Quantitative Analysis: To quantitatively measure the consistency of the distribution of different subregions, we used Kendall's coefficient of concordance (W) for u_i to access the agreement of subregions based on rank order, which ranges from 0 (no agreement) to 1 (complete agreement). We first calculated W for each subregion of twenty-five subjects in each session, as shown in Table S4. We observed that all P values were less than 0.001, indicating that each obtained subregion had a significant agreement among all subjects. Then we calculated W for each subregion of each subject in 3 sessions, as shown in Table S5. We observed that $88\%, 88\%$, and 80% of subjects had an agreement

Table S3

THE SIGNIFICANTLY CORRELATED REFERENCE ROIS WITH THE RIGHT PUTAMEN

	subregion 1	subregion 2	subregion 3
session 1	Rolandic_Oper_R Insula_L&R Amygdala_R Pallidum_L&R Thalamus_R Temporal_Sup_R	Parietal_Sup_L&R Fusiform_L&R SupraMarginal_L&R Paracentral_Lobule_L&R	Precentral_L&R Amygdala_L&R Postcentral_L&R Temporal_Sup_R
session 2	Rolandic_Oper_R Insula_L&R Pallidum_L&R Temporal_Sup_L&R	Lingual_L&R Fusiform_L&R Cerebellum_6_L&R	ParaHippocampal_L&R Amygdala_L&R Temporal_Pole_Sup_L&R Temporal_Mid_R
session 3	Rolandic_Oper_R Insula_L&R Cingulum_Mid_R Amygdala_R Pallidum_L&R Thalamus_R Temporal_Sup_L&R	Lingual_L Fusiform_L&R Paracentral_Lobule_L&R Cerebellum_4_5_R Cerebellum_6_L	Olfactory_L Hippocampus_L&R ParaHippocampal_L&R

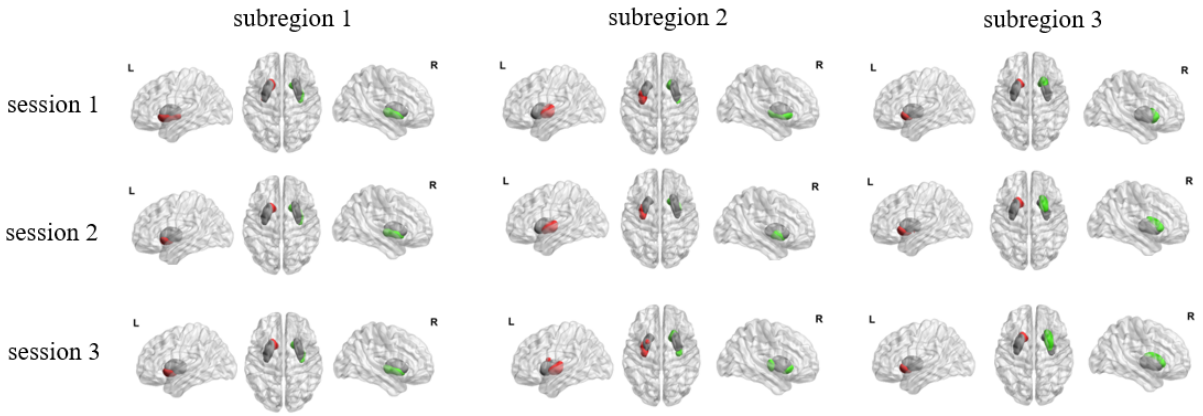

Figure S1. The hard parcellation results of one subject from three views (L, S, R). The red regions are subregions in the left Putamen and the green ones are subregions in the right Putamen.

among 3 sessions for subregions 1 to 3 in the left Putamen, respectively, and $96\%, 84\%$, and 84% in the right Putamen. Given the possible variability across the subjects, the results demonstrate that for most subjects, we can get consistent parcellation results among 3 sessions. The results demonstrate that the proposed model has superior reproducibility for joint functional brain subregion parcellation.

Further, we calculated the correlation coefficients r, which measured the functional connectivity

Table S4

KENDALL'S COEFFICIENT OF CONCORDANCE OF THE 25 INDIVIDUALS

	the left Putamen			the right Putamen		
	subregion 1	subregion 2	subregion 3	subregion 1	subregion 2	subregion 3
session 1	0.390*	0.535*	0.386*	0.540*	0.527*	0.377*
session 2	0.410*	0.457*	0.677*	0.591*	0.389*	0.399*
session 3	0.370*	0.421*	0.780*	0.499*	0.365*	0.392*

Null hypothesis is no agreement ($W = 0$). '*' represents that null hypothesis is rejected, with P value < 0.001.

Table S5

KENDALL'S COEFFICIENT OF CONCORDANCE OF THE 3 SESSIONS

subject	the left Putamen			the right Putamen		
	subregion 1	subregion 2	subregion 3	subregion 1	subregion 2	subregion 3
1	0.597**	0.883**	0.867**	0.940**	0.683**	0.399 (0.008)*
2	**0.312 (0.786)**	0.933**	0.834**	0.615**	**0.094 (1.000)**	0.475**
3	0.636**	0.751**	0.927**	0.781**	0.586**	0.502**
4	**0.311 (0.797)**	0.767**	0.711**	0.820**	**0.217 (1.000)**	0.488**
5	0.804**	0.472**	0.812**	0.453**	0.512**	0.579**
6	0.572**	0.442**	**0.223 (1.000)**	0.966**	0.877**	0.459**
7	0.436**	0.398 (0.011)*	**0.344 (0.336)**	0.780**	0.459**	**0.160 (1.000)**
8	0.889**	0.887**	0.623**	0.974**	0.599**	0.774**
9	0.723**	0.951**	0.529**	0.823**	0.781**	0.947**
10	0.921**	0.864**	0.709**	0.943**	0.884**	0.608**
11	0.488**	0.857**	0.654**	0.804**	0.386 (0.026)*	0.914**
12	0.467**	**0.219 (1.000)**	0.729**	0.540**	0.469**	0.776**
13	**0.366 (0.116)**	0.609**	**0.306 (0.841)**	0.960**	**0.216 (1.000)**	0.647**
14	0.864**	**0.217 (1.000)**	0.629**	0.383 (0.035)*	0.479**	**0.297 (0.920)**
15	0.511**	0.959**	0.491**	0.569**	0.471**	0.887**
16	0.654**	0.557**	0.706**	0.637**	0.705**	0.389 (0.022)*
17	0.715**	0.751**	0.934**	0.948**	0.894**	0.748**
18	0.659**	0.731**	0.575**	0.543**	0.595**	0.830**
19	0.695**	**0.326 (0.599)**	**0.310 (0.804)**	0.909**	0.456**	**0.183 (1.000)**
20	0.548**	0.417 (0.002)*	0.649**	0.877**	0.628**	0.590**
21	0.751**	0.861**	0.971**	0.504**	0.790**	0.5560**
22	0.598**	0.490**	0.871**	**0.228 (1.000)**	0.807**	0.483**
23	0.399 (0.010)*	0.707**	0.471**	0.576**	**0.308 (0.828)**	**0.359 (0.168)**
24	0.867**	0.918**	0.715**	0.992**	0.496**	0.751**
25	0.854**	0.652**	**0.142 (1.000)**	0.786**	0.447**	0.594**

Null hypothesis is no agreement ($W = 0$). P value is written in the brackets if it is larger than 0.001. '*' represents that null hypothesis is rejected, with P value < 0.05. '**' represents that null hypothesis is rejected, with P value < 0.001. The bold data indicate that null hypothesis is accepted.

Table S6

SUBREGIONAL HOMOGENEITY IN THE 3 SESSIONS (%)

	the left Putamen			the right Putamen		
	subregion 1	subregion 2	subregion 3	subregion 1	subregion 2	subregion 3
session 1	53.216	47.868	42.428	51.613	47.277	36.554
session 2	52.580	47.434	42.366	50.399	45.239	34.684
session 3	54.207	49.686	44.123	51.400	46.727	35.715

strength between subregions and reference ROIs. In session 1, the mean of r was $0.822, 0.433, 0.407$ for subregions 1 to 3 in the left Putamen, respectively, and $0.801, 0.478, 0.453$ in the right Putamen. In session 2, the result was $0.813, 0.439, 0.408$ for the left, respectively, and $0.797, 0.460, 0.442$ for the right. In session 3, the result was $0.816, 0.431, 0.414$ for the left, respectively, and $0.788, 0.449, 0.412$ for the right. The correlation coefficients decreased sequentially with the subregion index as expected, and the results were quite consistent in 3 sessions.

Finally, we investigated the validity of our parcellation. A pivotal marker of parcellation validity is the subregional homogeneity of functional signals. Regional homogeneity is defined as the variance explained by the first principal component of the data, which is estimated using principal component analysis (PCA). Homogeneity was respectively computed for each subject, and then averaged across all subjects to yield parcellation homogeneity for a subregion, referred to as subregional homogeneity. The results are shown in Table S6. There was no significant difference among the 3 sessions, and we observed that subregional homogeneity decreased along with the subregion index. This shows the strong validity of our model when dealing with functional subregion parcellation.

II. CLASSIFICATION AND REGRESSION EXPERIMENTS

To illustrate the clinical practice of our model, we performed disease prediction and severity prediction experiments on UBC data. We compared the results with those of JS-CCA (the second optimal method based on the simulation results) to evaluate the superiority of the proposed model.

A. Regression

We attempted to predict UPDRS-III scores of PD patients based on estimated subregional features obtained from the proposed model. The linear regression model was used, and leave-one-out cross validation was adopted (one subject as the testing set at a time and the others as the training set). The input data sets were the connectivity strength and homogeneity of each subregion. Similarly, we predicted UPDRS-III scores based on the subregional features obtained from JS-CCA. As shown in Fig. S2, based on our proposed model, the correlation coefficient between the predicted and

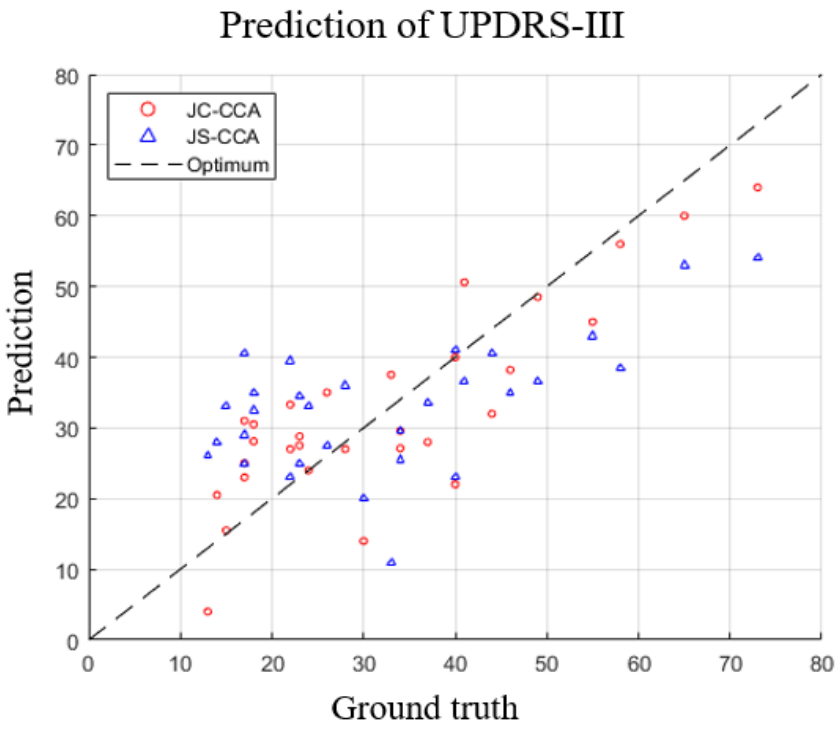

Figure S2. Prediction results of UPDRS-III. The correlation coefficient between the predicted and true UPDRS-III scores is 0.84 and 0.68 for JC-CCA and JS-CCA, respectively. The root mean square error (RMSE) between the predicted and true UPDRS-III scores is 8.61 and 12.73 for JC-CCA and JS-CCA, respectively.

true UPDRS-III scores is 0.84. Compared with JS-CCA, our proposed method yielded superior performance in predicting UPDRS-III scores, with a higher correlation coefficient and a lower root mean square error (RMSE). The results demonstrate that our proposed method can identify clinically important features and benefit disease severity prediction, validating its potential in clinical practice.

B. Classification

We further performed disease classification based on the estimated connectivity strength and homogeneity of each subregion. It classified whether a subject was a PD patient or not (PD: 1, HC: 0). Support vector machine (SVM) and linear discrimination analysis (LDA) were used separately, and leave-one-out cross validation was adopted. The confusion matrices are shown in Table S7 and Table S8. To evaluate the superiority of the proposed method, we compared its performance with that of JS-CCA (Table S9 and Table S10). The results demonstrated that SVM achieved better classification performances for both methods. Specifically, SVM based on JC-CCA obtained a classification accuracy of 84.5%, which was comparable with several previous studies [1], [2], [3], [4], while the classification accuracy using LDA based on JC-CCA was 69.0%. Compared with the features obtained from JS-CCA, the subregional features of JC-CCA better distinguished diseased populations,

Table S7

CONFUSION MATRIX OF SVM FOR JC-CCA

Truth \ Prediction	1	0
1	26	4
0	5	23

TPR = 86.7%, FPR = 17.9%, Accuracy Rate = 84.5%.

Table S8

CONFUSION MATRIX OF LDA FOR JC-CCA

Truth \ Prediction	1	0
1	29	9
0	9	19

TPR = 70.0%, FPR = 32.1%, Accuracy Rate = 69.0%.

indicating its potential in clinical practice.

It is worth noting that SVM and LDA may not be optimal classifiers for disease classification. The deep learning-based models and various extensions of SVM may achieve better performances. However, the focus of this work is the group parcellation problem in the native space. Here we want to provide an intuitive comparison with other models and illustrate the clinical potential of the proposed model. In our future work, we would further optimize the classifiers and adopt multimodal features.

III. ROIS SELECTED FOR UBC DATA

The 48 ROIs used in the UBC data are provided in Table S11.

Table S9

CONFUSION MATRIX OF SVM FOR JS-CCA

Truth \ Prediction	1	0
1	22	8
0	6	22

TPR = 73.3%, FPR = 21.4%, Accuracy Rate = 75.9%.

Table S10

CONFUSION MATRIX OF LDA FOR JS-CCA

Truth \ Prediction	1	0
1	19	11
0	10	18

TPR = 63.3%, FPR = 35.7%, Accuracy Rate = 63.8%.

Table S11

THE 48 ROIS SELECTED IN UBC DATA

No.	Name	No.	Name
1	Left-Cerebellum-Cortex	25	ctx_lh_G_temp_sup-Lateral
2	Left-Thalamus-Proper	26	ctx_lh_G_temp_sup-Plan_polar
3	Left-Caudate	27	ctx_rh_G_temp_sup-Lateral
4	Left-Putamen	28	ctx_rh_G_temp_sup-Plan_polar
5	Left-Pallidum	29	ctx_lh_G_temp_sup-Plan_tempo
6	Right-Cerebellum-Cortex	30	ctx_rh_G_temp_sup-Plan_tempo
7	Right-Thalamus-Proper	31	ctx_lh_G_and_S_cingul-Ant
8	Right-Caudate	32	ctx_rh_G_and_S_cingul-Ant
9	Right-Putamen	33	ctx_lh_G_cingul-Post-dorsal
10	Right-Pallidum	34	ctx_lh_G_cingul-Post-ventral
11	ctx_lh_precuneus	35	ctx_rh_G_cingul-Post-dorsal
12	ctx_rh_precuneus	36	ctx_rh_G_cingul-Post-ventral
13	ctx_lh_insula	37	R_M1
14	ctx_rh_insula	38	L_M1
15	ctx_lh_G_front_middle	39	R_S1
16	ctx_rh_G_front_middle	40	L_S1
17	ctx_lh_G_pariet_inf-Angular	41	R_SMA_proper
18	ctx_rh_G_pariet_inf-Angular	42	L_SMA_proper
19	ctx_lh_G_pariet_inf-Supramar	43	R_Pre_SMA
20	ctx_rh_G_pariet_inf-Supramar	44	L_Pre_SMA
21	ctx_lh_G_parietal_sup	45	R_PMd
22	ctx_rh_G_parietal_sup	46	L_PMd
23	ctx_lh_G_temp_sup-G_T_transv	47	R_PMv
24	ctx_rh_G_temp_sup-G_T_transv	48	L_PMv

REFERENCES

[1] L. Salamanca, N. Vlassis, N. Diederich, F. Bernard, and A. Skupin, "Improved Parkinson's disease classification from diffusion MRI data by Fisher vector descriptors," in *International Conference on Medical Image Computing and Computer-Assisted Intervention*. Springer, 2015, pp. 119–126.

[2] H. Lei, Z. Huang, J. Zhang, Z. Yang, E.-L. Tan, F. Zhou, and B. Lei, "Joint detection and clinical score prediction in Parkinson's disease via multi-modal sparse learning," *Expert Systems with Applications*, vol. 80, pp. 284–296, 2017.

[3] J. Cai, A. Liu, T. Mi, S. Garg, W. Trappe, M. J. McKeown, and Z. J. Wang, "Dynamic graph theoretical analysis of functional connectivity in Parkinson's disease: The importance of Fiedler value," *IEEE journal of biomedical and health informatics*, vol. 23, no. 4, pp. 1720–1729, 2018.

[4] H. Gunduz, "Deep learning-based Parkinson's disease classification using vocal feature sets," *IEEE Access*, vol. 7, pp. 115 540–115 551, 2019.